Fizika Nizkikh Temperatur, 2010, v. 36, No. 5, p. 484–494

Stabilization of H and D atoms in krypton–helium nanocondensates

R.E. Boltnev

Branch of Institute of Energy Problems of Chemical Physics, Chernogolovka, Moscow Region 142432, Russia
E-mail: boltnev@binep.ac.ru

V.V. Khmelenko and D.M. Lee

Laboratory of Atomic and Solid State Physics, H8, Clark Hall, Cornell University, Ithaca, New York 14853, USA
Department of Physics and Astronomy, Texas A&M University, College Station, TX, 77845, USA

Received December 18, 2009, revised January 13, 2010

Impurity–helium condensates formed by krypton nanoclusters containing atoms and molecules of hydrogen isotopes have been studied via an electron spin resonance (ESR) technique. Analysis of the ESR spectra has shown that most of the H and D atoms reside on the surfaces of Kr nanoclusters. Very large average concentrations have been obtained for H atoms ($1.2\cdot10^{19}$ cm^{-3}) and D atoms ($3.3\cdot10^{19}$ cm^{-3}) in these experiments. For the highest concentration of D atoms stabilized in the Kr–He sample, line narrowing has been observed. Exchange tunneling reactions have been studied in Kr–He sample containing H and D atoms.

PACS: 76.30.Rn Free radicals;
67.80.dk Magnetic properties, phases, and NMR;
67.80.fh Atomic hydrogen and isotopes.

Keywords: free radicals, impurity nanoclusters, condensed helium, ESR spectroscopy.

1. Introduction

Cryogenic matrices are widely used for spectroscopic studies of highly reactive or transient species. Such rare gases as neon, argon and krypton as well as molecular nitrogen and hydrogen are traditional inert host materials for matrix isolation. Helium, the most inert substance, was for more than 30 years the one exception among the rare gases to serve as an effective medium for matrix isolation. Spectroscopy of impurity atoms/molecules in condensed helium has not had a very long history. Due to unique properties of condensed (solid and liquid) helium there was no straightforward way to introduce single impurity atoms (molecules) into the bulk. Among the first observations of fine impurity particles in liquid helium (LHe) was that of Savich and Shalnikov in 1946 [1]. Later, spectra of molecular nitrogen and oxygen were detected from liquid helium upon excitation by a ^{210}Po α-particle source [2]. The application of pulsed laser ablation for reliably doping liquid helium with single atoms and small clusters [3] is now in use in many experimental groups and the results were reviewed in detail in Refs. 4, 5. Extended spectroscopic studies of atoms and molecules trapped in large LHe droplets have been carried out since the 1990s [6,7].

Cryogenic matrices were also used to try to achieve high enough concentrations of radicals to store large amounts of chemical energy for some practical applications, such as a possible more effective rocket fuel [8]. Particular efforts were made to stabilize hydrogen atoms since they have highest ratio of recombination energy to recombination product mass. Nevertheless, researchers in the 1950s were never able to obtain concentrations exceeding about 0.01%, far below the criterion for any practical energy storage applications. So far the highest densities of H atoms in bulk (molecular matrices of hydrogen isotopes), $7\cdot10^{18}$ cm^{-3}, were obtained at $T = 1.4$ K [9]. Recently, higher densities of atomic hydrogen (up to $2\cdot10^{19}$ cm^{-3}) were achieved in solid H_2 films below 1 K [10]. From this point of view, impurity–helium condensates (IHCs) are very promising nanomaterials for creation of new high density energetic materials. IHCs form in superfluid ^{4}He (He II) upon condensation of a helium gas jet containing ~1% of admixtures (molecular and/or atomic hydrogen, nitrogen or oxygen, and/or atoms of neon, argon, krypton, xenon). This technique was invented and developed in Chernogolovka to stabilize and study free radicals in superfluid helium in the 70's [11].

In this intermediate review we summarize the recent results of X band (9 GHz) electron spin resonance (ESR) experiments performed on H and D atoms in impurity–helium condensates mainly composed of Kr nanoclusters. A discussion of some of the work discussed herein has also appeared in other publications [12,13]. Macroscopic samples (volume ~cm^3) of IHCs containing the record average concentration of H and D atoms, $1.2\cdot10^{19}$ and $3.3\cdot10^{19}$ per cm^3, respectively, were created.

2. Experimental techniques and data processing

IHCs with stabilized H and/or D atoms for ESR investigations were prepared *in situ* in a Janis cryostat by sending a jet of helium gas containing 0.5 % of impurities (Kr atoms and H_2, D_2 or HD molecules) through a radiofrequency electric discharge (f = 52 MHz, P = 70 W) onto the surface of He II contained in a small beaker sitting above a main helium bath at $T \approx 1.5$ K (Fig. 1). The distance between the orifice of the gas jet source and the surface of He II was 2 cm [14,15]. During collection, a fountain pump in the main helium bath was used to maintain the helium level in the beaker. Upon cooling the jet by cold helium gas, krypton clusters were formed which contain atoms and molecules of hydrogen isotopes on their surfaces and in their interiors. The jet penetrated the surface of liquid helium and a macroscopic snowlike semitransparent material was created. The collection beaker consisted of a funnel connected to a thin cylindrical tube at the bottom. Teflon blades were used to scrape off any sample adhering to the funnel. This material fell down through the liquid ^{4}He to form a porous sample at the bottom of the beaker. To prepare the IHC sample a jet with a flux of $\approx 5\cdot10^{19}$ atoms and molecules per second was condensed during a 10 min period. Immediately after preparation at 1.5 K, the IHC sample was cooled down to 1.35 K by turning off the discharge, stopping the gas flux, and pumping harder on the main He bath. The beaker containing the fresh «as-prepared» sample then was lowered into the ESR cavity, which was situated at the bottom of the cryostat in the homogeneous field region of a Varian 7800 electromagnet. The volume occupied by the sample inside the cavity was 0.35 cm^3. The homemade cylindrical cavity was operated in the TE_{011} mode. ESR signals were recorded by using a continuous wave reflection homodyne spectrometer «Varian E-4» with operating frequency near 9.07 GHz. The microwave carrier frequency was measured by using a frequency counter «EIP 545» while the field was swept through each resonance. Derivatives of the ESR absorption lines were detected at the magnetic field values in the region of ≈ 3200 G by the addition of a small amplitude modulation field oscillating at 100 kHz.

To determine the average concentration, n, as well as the spectroscopic constants (the hyperfine structure constants, A, and g-factors) of hydrogen (deuterium) atoms stabilized in IHC samples, each of the detected lines was fitted by a set of derivatives of Gaussian and Lorentzian functions. The average concentration of H (D) atoms in a sample was determined from the amplitudes and widths of the fitting curves. The number of unpaired spins associated with each of the fitting curves was obtained by comparison with the signals from a ruby crystal with a known number of spins emplaced in the cavity. Adding the number of spins corresponding to all hyperfine components (a doublet for H atoms and a triplet for D atoms) and dividing by the sample volume gave the average concentration of H (D) atoms in the sample. The ruby crystal used as a secondary standard to measure the average concentration of the spins was attached permanently to the bottom of the microwave cavity. The calibration of the absolute value of the number of spins in the ruby crystal was in turn accomplished by using a standard organic diphenyl-picrylhydrazil (DPPH)

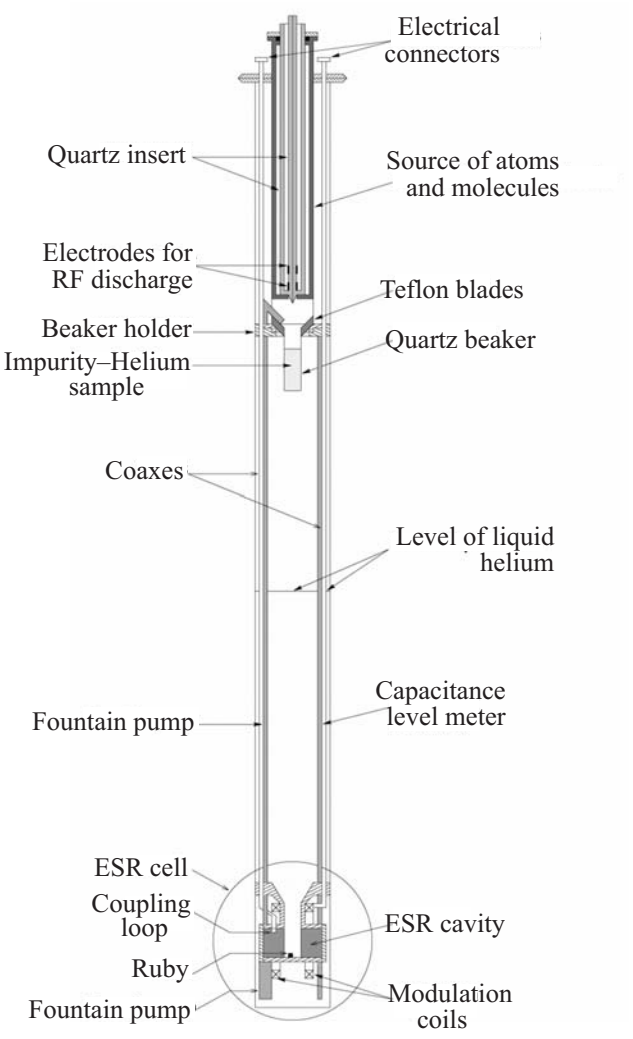

Fig. 1. Scheme of low-temperature insert for ESR spectroscopy of radicals stabilized in IHC samples.

sample with a known number ($2.43 \cdot 10^{17}$) of spins. The calibration measurements were carried out at T = 1.35 K and T = 1.8 K. A Lake Shore germanium resistance thermometer calibrated for the temperature range 1–60 K was placed next to the ESR cavity.

The positions of fitting curves and the resonance frequencies were used to calculate the hyperfine constants A and the g-factors by inverting the Breit–Rabi equation [16]. A nuclear magnetic resonance (NMR) magnetometer «Sentec 1001» was used for precise measurements of magnetic field. The distribution of the magnetic field in the electromagnet was mapped by removing the cryostat from the magnet gap and moving the NMR probe throughout the gap. The relative homogeneity of the magnetic field at the value 3200 G over the volume of the sample was $3.13 \cdot 10^{-6}$. From the measured ESR signal of DPPH with known g-factor (g = 2.0037) at the temperature 1.35 K, the difference of the magnetic field between the position of the sample in the center of magnet inside the cryostat and the position of the NMR probe located outside cryostat was determined to be 1.58 G. This value has been taken into account in the analysis of all ESR spectra of H and D atoms recorded at low temperatures. By reducing the supply of liquid helium into the variable temperature insert of the cryostat we lowered the level of liquid helium and were able to warm up the IHC sample in the ESR cavity. Following observations at 1.35 K, the IHC samples were slowly heated to temperatures between 10 and 14.5 K and then cooled back down to 1.35 K. A home-made temperature controller was used to control and stabilize the temperature of the sample. As a result of this annealing process, the concentration of atoms was greatly reduced as they recombined into molecules.

3. Results and discussion

From our earlier x-ray experiments we know the structure of krypton–helium condensates prepared from gas mixtures [Kr]:[He] ≈ 1:200. They possess an aerogel-like structure formed by krypton hico nanoclusters (mean size of 5.4 nm) covered with a solid helium layer [17,18]. The average densities of as-prepared Kr–He samples were determined by x-ray absorption measurements and were found to be ~10^{19} cm^{-3}, about 0.1% of the bulk Kr density. Much higher densities can be obtained by mechanical compression or annealing of the samples [19]. The hico clusters are perfect icosahedral clusters with an hcp-like overlayer above all the (111) faces of the icosahedron [20]. The hico clusters exhibit the smallest normalized fraction of the surface atoms, and therefore are the most spherical clusters. This might indicate that the clusters first form in the cold helium gas as liquid droplets and then quickly freeze, preserving their nearly spherical shape [18].

For the case of cooling the hydrogen (deuterium)–krypton–helium gas jet, we expect the formation of nanoclusters of nearly pure Kr at higher temperatures. This occurs because of the strong van der Waals forces between the Kr atoms [18]. Then, at lower temperatures, closer to the surface of He II in the beaker, the more weakly attracted H (D) atoms, H_2 (D_2) molecules, and He atoms bind to the Kr cluster surfaces. So we will call the samples under study krypton–helium condensates, because of principal role of krypton atoms in IHC formation, regardless of a significant content of hydrogen (deuterium) in some of the samples.

3.1. H atoms in krypton–helium condensates

We first discuss ESR signals of H atoms obtained from three IHC samples prepared from different initial gas mixtures [H_2]:[Kr]:[He] = 1:1:200, [H_2]:[Kr]:[He] = 1:5:1200 and [H_2]:[Kr]:[He] = 1:50:10,000 (Fig. 2). The high field line (HFL) and low field line (LFL) of atomic hydrogen were separated by about 508 G. A small shoulder or bump can be seen on the right hand side of the LFL line (at ≈ 2962.5 G) in each of the three panels. The HFL spectra do not exhibit this shoulder. The shoulder always occurs at or close to the same applied field in each of the three spectra, whereas the main low field lines are shifted relative to one another for the three

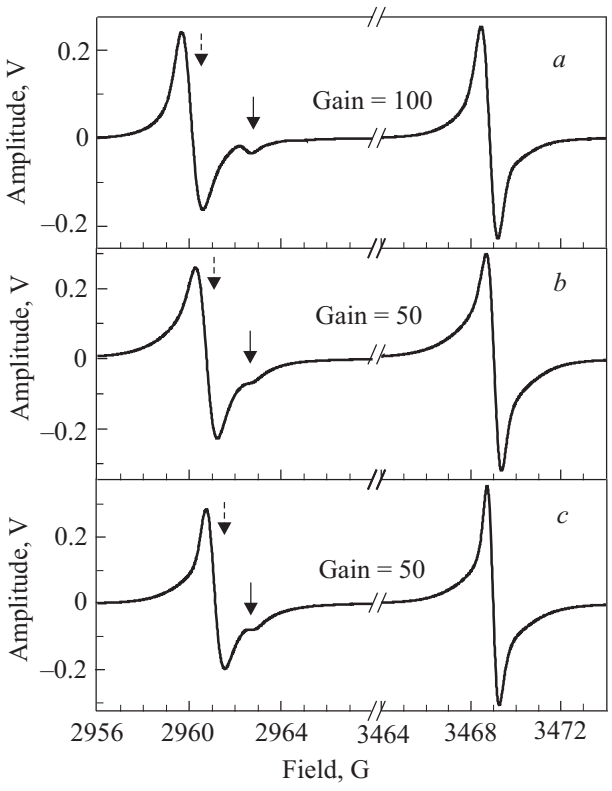

Fig. 2. ESR spectra of H atoms in as-prepared H–Kr–He samples at 1.35 K. The solid arrows and the dashed arrows point to the bump positions and the LFL centers, respectively. Samples were prepared from gas mixtures with the ratios [H_2]:[Kr]:[He] = 1:1:200 (*a*), [H_2]:[Kr]:[He] = 1:5:1200 (*b*), and [H_2]:[Kr]:[He] = 1:50:10,000 (*c*).

different cases shown in panels (*a*), (*b*) and (*c*). The main LFLs are seen to shift to the right as the H_2 content in the make-up gas is reduced relative to the Kr and He gases. The high field lines do not shift positions significantly as we go through the sequence (*a*), (*b*), (*c*).

The ESR spectra for the low and high field lines were each fitted by one Gaussian and two Lorentzian lines [12]. For a proper fit, all three of these curves were required. In our first report on this topic we used for this purpose another fitting curve set consisting of three Lorentzian lines [21]. Nevertheless, better fitting results achieved with the new set along with observation of satellites (Fig. 3) fitted by the Gaussian line have confirmed the new choice. Very weak satellite peaks can be seen around the hyperfine lines of H atoms for IHC samples prepared from gas mixtures with the highest hydrogen contents, $[H_2]:[Kr]:[He] = 1:1:200$ and $[H_2]:[Kr]:[He] = 1:1:400$ only. The HFL spectrum of H atoms together with the satellites (splitting of 5.3 G and the amplitude ratio $I_{satellite}/I_{main}$ of about 0.008) and Gaussian fit lines are shown in Fig. 3 for the former sample. The satellite lines were shown to be associated with mutual spin flips of the H atom electron with nuclei of the ortho molecules [22]. The satellites and Gaussian line for the high field lines have the same line width values (≈0.8 G). The satellites around the LFL (with a splitting of 4.6 G) were disturbed much more due to the presence of the bump. The fractions of H atoms associated with the Gaussian lines were the largest for these samples and equal to 13 and 11%, respectively. The fractions of H atoms corresponding to the broad Lorentzian were about 80% for these samples while for the other samples under study, they were equal ≈ 90%.

The fitting for one set of spectra, corresponding to the H atoms in the sample prepared from the gas mixture

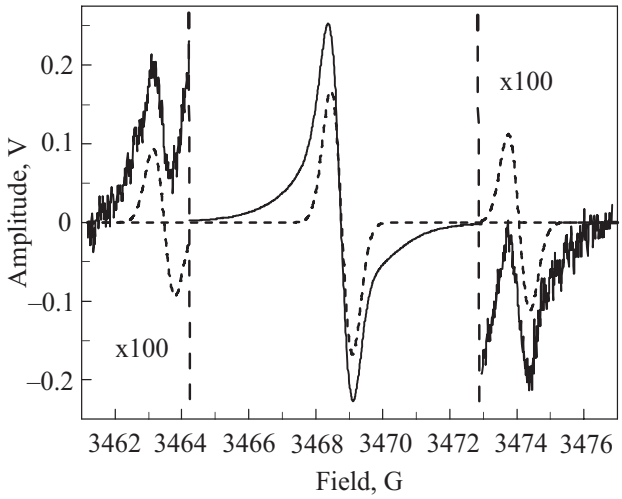

Fig. 3. A high field main line of atomic hydrogen with satellite lines (solid lines). Satellites of the HFL correspond to the Gaussian fitting line of the main HFL. Gaussian fitting lines are presented by dashed lines. The sample was prepared from the gas mixture $[H_2]:[Kr]:[He] = 1:1:200$.

$[H_2]:[He]:[Kr] = 1:50:10{,}000$ in panel (*c*) in Fig. 2 is illustrated in Fig. 4. Curve *1* is the Gaussian line and curves *2* and *3* are the Lorentzian lines. Corresponding curves calculated for the other two panels (*a* and *b*) in Fig. 2 are identified as *1a*, *2a*, *3a* and *1b*, *2b*, *3b*. A figure showing these latter curves is not provided, since the fitting procedure and agreement with the data is similar to that shown in Fig. 4. In Table 1 we list the values of the line widths, the *g*-factors and the hyperfine structure constants *A* obtained for H atoms from the experimental data for each of the different curves. The data for H atoms in gas phase, in solid H_2 and in Kr matrices are listed also for comparison.

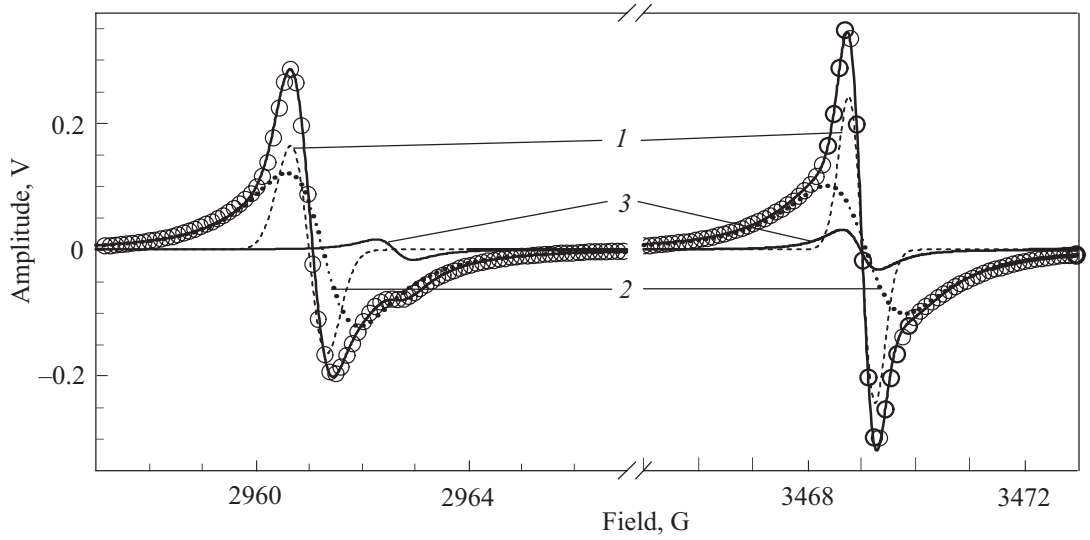

Fig. 4. Experimental ESR spectra of H atoms for the as-prepared H–Kr–He sample (open circles) shown in Fig. 2,*c* and sets (one set for the LFL and one set for the HFL) of three fitting curves (*1* — Gaussians are dashed lines, *2* — broad and *3* — narrow Lorentzians are dotted and thin lines, respectively) and the sums of fitting curves (thick lines).

Table 1. Hyperfine structure constants, A, g-factors, and line widths for ESR spectra of H atoms in as-prepared (curves *1*–*3*) and annealed (curves *4* and *5*) Kr–He condensates, in the gas phase, in solid H_2 and in Kr matrices

Matrix	A, MHz	$\Delta A/A_{free}$,%	g-factor	Line width,G
H–Kr–He, curve *1a*	1416.33(20)	−0.29	2.00228(5)	0.8
H–Kr–He, curve *2a*	1415.49(62)	−0.35	2.00220(16)	2.1
H–Kr–He, curve *3a*	1408.74(43)	−0.82	2.00176(11)	1.2
H–Kr–He, curve *4a*	1409.60(20)	−0.76	2.00160(5)	3.3
H–Kr–He, curve *5a*	1407.88(43)	−0.88	2.00178(11)	0.6
H–Kr–He, curve *1b*	1415.15	−0.37	2.00209	0.8
H–Kr–He, curve *2b*	1414.84	−0.39	2.00212	2.4
H–Kr–He, curve *3b*	1412.26	−0.57	2.00131	1.6
H–Kr–He, curve *4b*	1412.27	−0.57	2.00134	2.3
H–Kr–He, curve *5b*	1407.96	−0.876	2.00182	0.46
H–Kr–He. curve *1*	1414.71	−0.40	2.00199	0.7
H–Kr–He, curve *2*	1414.09	−0.45	2.00192	2.36
H–Kr–He, curve *3*	1409.935	−0.74	2.00158	1.1
H–Kr–He, curve *4*	1408.23	−0.86	2.00176	2.22
H–Kr–He, curve *5*	1407.63	−0.9	2.00177	0.41
Gas phase [23,24]	1420.40573(5)	0	2.002256(24)	–
H_2 [25]	1417.13(45)	−0.23	2.00243(8)	–
Kr (subst.) [26]	1411.799(30)	−0.61	2.00179(8)	–
Kr (subst.) [27]	1408.97	–0.805	2.00164(12)	–
Kr (subst.) [28]	1409	−0.80	2.0013	–
Kr (interst.) [26]	1427.06(280)	+0.47	1.99967(31)	–

Evolution of the ESR spectra of H atoms stabilized in a Kr–He sample upon annealing is shown in Fig. 5. Comparison of the spectra in Fig. 5 provides an important clue regarding the placement of the H atoms in the samples before and after annealing. The fact that the signal associated with the bump (or more precisely curve *3* of Fig. 4) corresponds to the *remaining* LFL signal after annealing led to the working hypothesis that the bump could be associated with H atoms embedded inside the Kr nanoclusters.

In accordance with this hypothesis, it was found that the entire large main LFL disappears upon annealing. The vanishing of the main LFL is attributed to the recombination of H atoms trapped in an H_2 layer at the Kr cluster surfaces. Further justification of the working hypothesis is provided in the discussion of Table 1 given below. Comparison of the relative sizes of the bumps and the main lines of as-prepared samples indicated that most of the H atom population is trapped on the surfaces (≈ 95%) and the remainder is trapped in the interior of the Kr clusters.

The average concentrations of H atoms obtained in the as-prepared IHC samples shown in Fig. 2 were $1.4\cdot10^{18}$, $3\cdot10^{18}$, and $3.2\cdot10^{18}$ cm^{-3}, for the samples prepared from initial gas mixtures $[H_2]$:[Kr]:[He] = 1:1:200, $[H_2]$:[Kr]:[He] = 1:5:1200 and $[H_2]$:[Kr]:[He] = 1:50:10,000, respectively. The last sample shrank upon warming up to 3.5 K and lowering the He II level in the ESR cavity. Only a small part of the porous sample collected in cylindrical part of the beaker filled the cavity volume before annealing. During annealing, the Kr

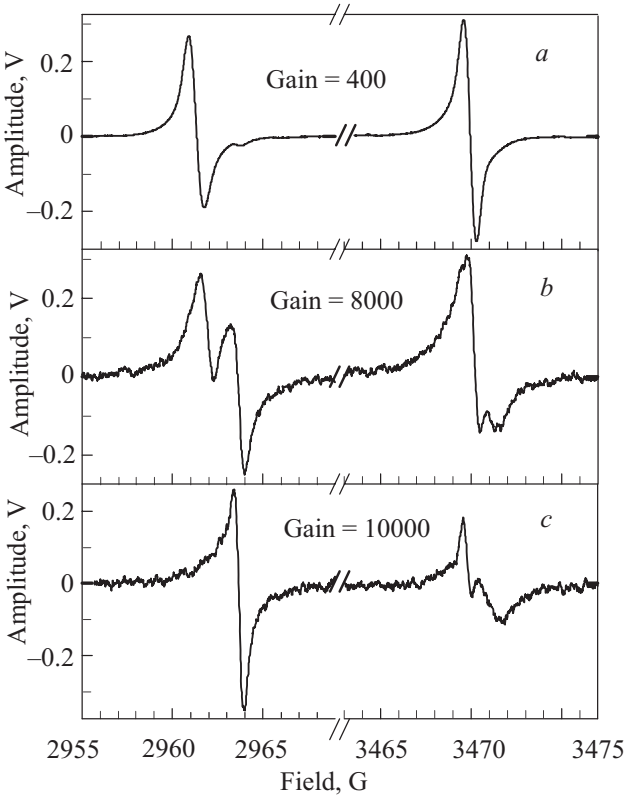

Fig. 5. Evolution of the ESR spectra of H atoms in Kr–He sample prepared from the gas mixture $[H_2]$:[Kr]:[He] = 1:1:400: as-prepared sample (*a*); the sample at T = 3 K (*b*) and T = 5 K (*c*).

clusters of the sample moved closer together and more hydrogen atoms entered the sensitive zone of the cavity. We observed the ESR signal amplitude increase while the other parameters of the ESR spectra (line widths, shapes and positions) kept their values. As a result of the sample shrinking the average concentration was increased to $1.2 \cdot 10^{19}$ cm^{-3}. For a typical Kr cluster size of 5.4 nm (corresponding to about 1800 atoms per cluster) [18], the number of clusters ($\sim 10^{17}$), their total surface area ($\sim 10^{19}$ nm^2), and the local concentration (~ 1 atom per 2 nm^2) of H atoms can be estimated from a knowledge of the total number of Kr atoms injected during the sample preparation ($\approx 2 \cdot 10^{20}$). For this highest local H concentration, the separation between H atoms on the cluster surfaces was estimated to be 1.4 nm [12]. This separation can be compared with the thermal de Broglie length of free H atoms at 1.3 K which is equal to 1.5 nm.

Comparison of the three different curves in Fig. 2 corresponding to three different initial gas mixtures provides additional information. As the relative H atom concentration in the gas mixture decreases, the main LFL tends to shift to the right, towards the bump. This indicates that for the case of Fig. 2,*a*, the H atoms are trapped in a thick H_2 film corresponding to relatively weak interactions with the Kr substrate. As we progress to Figs. 2,*b* and 2,*c*, the thickness of H_2 layer decreases and the H atoms interact more and more with the Kr substrate, leading to a shift of the main LFL to the right, closer to the position of the ESR line of H atoms in a Kr matrix. For determination of the exact thickness of the H_2 layers, additional experiments are needed. The above interpretations are confirmed by referring to Table 1. From Table 1 it can be seen that the *g* and *A* values obtained from Fig. 2,*a* corresponding to curves *1a* and *2a* agree most closely with the values for H atoms trapped in solid H_2 whereas curve 3a corresponds to H atoms embedded in solid Kr. As we progress to Fig. 2,*b*, curves *1b* and *2b* show that the influence of the Kr substrate becomes stronger. This progression indicates that the H_2 coatings on the clusters became thinner as the H_2 concentration in the make-up gas became more dilute. In contrast, curves *3a*, *3b* and *3* always remained at the position corresponding to H atoms trapped in solid Kr.

Figure 6 shows the ESR spectra of the annealed sample that were shown in Fig. 4 before annealing took place. We can see the shoulder or bump on the LFL for as-prepared samples occurs close to the value of the magnetic field obtained for the LFLs of the annealed sample. After annealing took place, both the *remaining* LFL and HFL could be represented by superposition of a broad Lorentzian line (*4*) and a narrow Gaussian line (*5*). The values of the hyperfine structure constants, *A*, and *g*-factors for H atoms in the annealed samples confirm that the atoms are located in krypton matrix.

There was no direct relation between the hydrogen content in a gas mixture and the number of H atoms stabilized in the sample formed from this mixture. Populations of H atoms in the samples prepared from gas mixtures rich in hydrogen decayed with time at the lowest temperature. Figure 7 shows the dependence of the H atom concentrations on time for two samples prepared from initial gas ratios of [H_2]:[Kr]:[He] = 1:1:200 (solid circles) and [H_2]:[Kr]:[He] = 1:50:10,000 (solid squares). The H atom populations for the former sample decays slowly. A linear dependence of the reciprocal concentration of H atoms on time would indicate a second-order recombination process for the H atoms. To obtain the recombination rate constant $K_H(T)$, we used the equation $K_H(T) = (2n_0\tau_{1/2})^{-1}$, where n_0 is

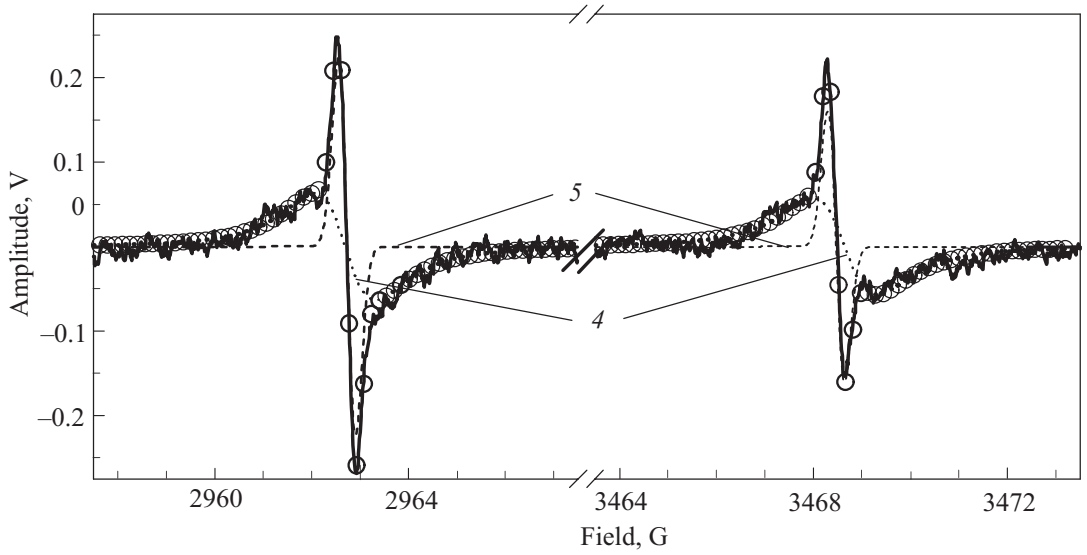

Fig. 6. Experimental ESR spectra of H atoms for an annealed H–Kr–He sample (thick lines) shown in Fig. 2,*c* and sets (one set for the LFL and one set for the HFL) of two fitting curves (*4* — Lorentzian and *5* — Gaussian are dotted and dashed lines, respectively) and the sums of fitting curves (open circles).

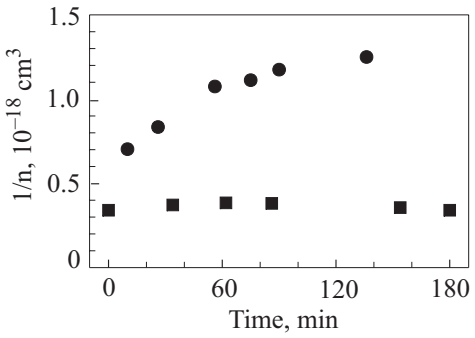

Fig. 7. Time dependences of the reciprocal H atom concentrations in samples prepared from $[H_2]$:[Kr]:[He] = 1:1:200 (solid circles) and $[H_2]$:[Kr]:[He] = 1:50:10,000 (solid squares) gas mixtures.

the initial concentration of H atoms and $\tau_{1/2}$ is the time needed to halve the initial concentration. With an initial concentration $n_0 = 1.4 \cdot 10^{18}$ cm^{-3}, we found a value of $\tau_{1/2} =$ = 161 min, leading to a rate constant of H atom recombination $K_H(1.35\ \text{K}) = 3.7 \cdot 10^{-23}$ cm^3/s. The H atoms are embedded in a thick H_2 film and therefore have enough mobility for recombination. On other hand, no decay was observed for the latter sample in which the H atoms are embedded in a thin film and are therefore very close to the Kr cluster substrate. The Kr surface binding would tend to retard recombination.

We find that the efficiency of stabilization of H atoms changes drastically for different gas mixtures. For example, for a gas mixture with a ratio $[H_2]$:[Kr]:[He]=1:1:400, the efficiency of H atom capture is only 0.13 % (and the average concentration $6 \cdot 10^{17}$ cm^{-3}), whereas for a gas mixture with a ratio $[H_2]$:[Kr]:[He]=1:50:10,000, the efficiency of H atom capture is 64% (and the average concentration $3.2 \cdot 10^{18}$ cm^{-3}). The high capture rate and *absence* of recombination of H atoms for this latter sample indicates that a large fraction of the hydrogen atoms in the layer covering Kr nanoclusters surfaces are atomic-free radicals bound directly to the Kr substrate rather than partners in H_2 molecules. Some of the remaining sites on the Kr clusters surfaces are occupied by He atoms.

3.2. D atoms in krypton–helium condensates

During the course of this work, experiments were also performed on krypton–helium condensates containing deuterium molecules and deuterium atoms. Typical ESR spectra of deuterium atoms for an as-prepared sample (a gas mixture $[D_2]$:[Kr]:[He] = 1:5:1200) are shown in Fig. 8, along with fitting curves. Since the nuclear spin of the deuteron is $I = 1$, there are three ESR components in the spectrum. The hyperfine components of D atoms are more symmetrical than the components of H atoms. Each of these components was fitted by a narrow (line width of ≈ 2 G) and a broad (line width of ≈ 5.5 G) Lorentzians, curves *6* and *7* of Fig. 8, respectively. The line width 5.5 G was the largest one observed in our experiments with D atoms indicating a large amount of dipolar broadening. For comparison, the largest line width 2.5 G was observed in our experiments with H atoms.

Deuterium atom ESR spectra for each of the samples under study were fitted as a rule (with one exception) by two Lorentzian curves. The exception was a Kr–He sample with the highest average concentration of D atoms $3.3 \cdot 10^{19}$ cm^{-3} (see Fig. 9). We can see some sharpening of every triplet component as compared to that at Fig. 8. Three fitting curves were needed to simulate the ESR spectra presented in Fig. 9: in addition to broad and narrow Lorentzians we had to use a sharp Gaussian (line width about 0.6 G). There are clear

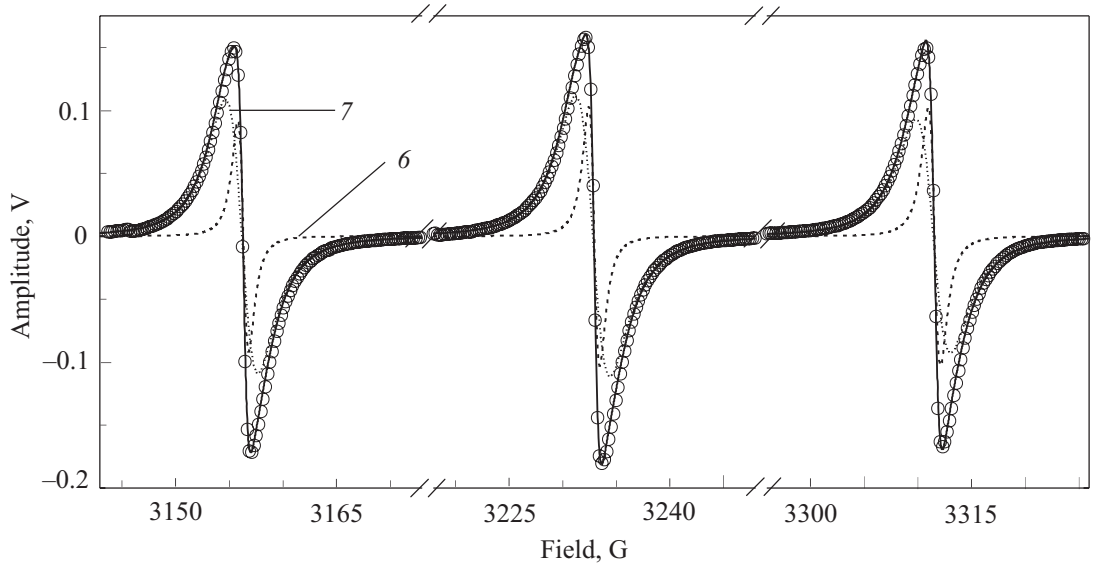

Fig. 8. Experimental ESR spectra of D atoms (open circles) in as-prepared Kr–He samples at 1.35 K (*6* — narrow Lorentzian, *7* — broad Lorentzian, the sum of the fitting curves — thick line). Sample was prepared from a gas mixture with the ratio $[D_2]$:[Kr]:[He] = 1:5:1200.

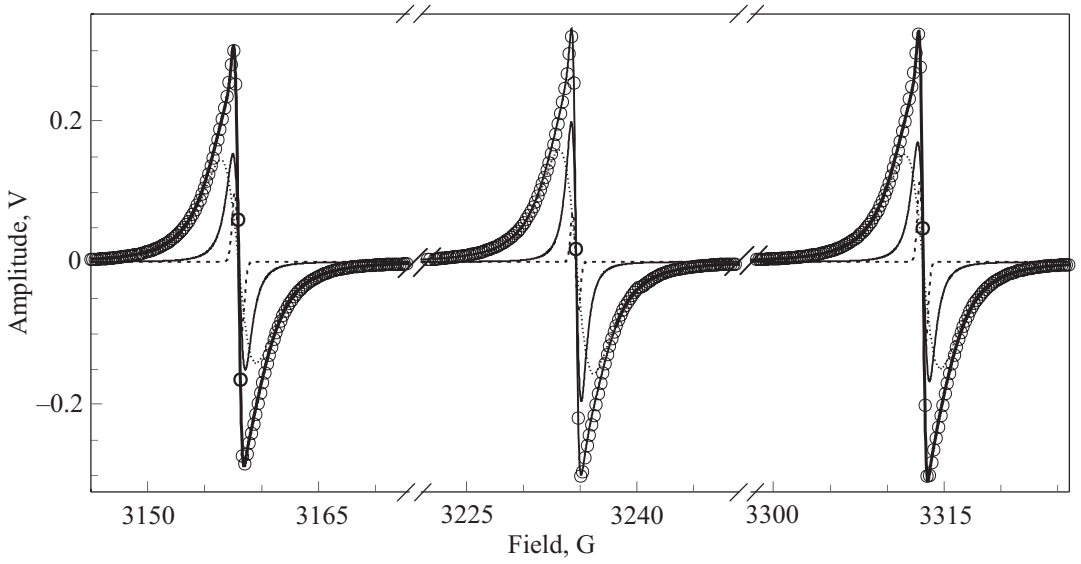

Fig. 9. Experimental ESR spectra of D atoms (open circles) in as-prepared Kr–He sample with the highest achieved average concentration of atoms ($3.3\cdot10^{19}$ cm^{-3}) at 1.35 K with 3 fitting curves for each hyperfine component: narrow Lorentzian — thin line, broad Lorentzian — dotted line, sharp Gaussian — dashed line, fit result — thick line).

differences with the ESR spectra of H atoms: we did not observe a bump in the ESR spectra in experiments with D atoms, and the hyperfine structure constants and *g*-factor values are almost the same for all fitting curves (Table 2) due to small relative shifts (less than 0.2 G) of the fitting curve positions for all the hyperfine components. Moreover there is no dependence of the hyperfine structure constant and *g*-factor values of D atoms on deuterium content in gas mixture used to form the Kr–He sample.

Table 2. Hyperfine structure constants, *A*, and *g*-factors for D atoms in Kr–He condensate, in the gas phase, in solid D_2 and in Kr matrices

Matrix	*A*, MHz	$\Delta A/A_{free}$,%	*g*-factor
D–Kr–He, curve *6*	217.448	−0.37	2.00198
D–Kr–He, curve *7*	217.4507	−0.37	2.00197
D–Kr–He (after annealing)	216.329	−0.883	2.00188
Gas phase [29–31]	218.25601(20)	0	2.002256(24)
D_2 [32]	217.71(18)	−0.25	2.00231(8)
D_2 [33]	217.607	−0.29	2.002202
Kr (subst.) [34]	216.30	−0.896	2.0015
Kr (interst.) [34]	219.8	+0.7	1.9997

A coincidence of the hyperfine structure constants and *g*-factor values for all the samples studied points to the same environment for each of the different populations of D atoms corresponding to different fitting curves. By comparing the values of these constants with the data known from the literature (see Table 2) it was found that all the D atoms reside in solid D_2 layers on the Kr nanocluster surfaces before annealing, in good agreement with the case for H discussed above. After annealing the remaining D atoms were embedded in the Kr clusters.

Estimations of the lower limit of the local (surface) density of D atoms in as-prepared samples can be made on the basis of the known numbers of spins contained in the sample ($\sim10^{19}$) and the Kr atoms entering the beaker during the sample preparation ($\sim 10^{20}$). Keeping in mind the characteristic size of Kr clusters forming krypton–helium condensates [18] (5.4 nm or about 2000 atoms per cluster) and the density of clusters ($\sim10^{17}$ cm^{-3}), it is easy to find the total surface area of the clusters and, correspondingly, the surface density of D atoms ~1 at./nm^2 for the case of one layer allocation. For such a high density of spins, exchange interactions may play a substantial role, possibly leading to exchange narrowing of the ESR lines.

The line widths of fitting curves for Kr–He condensates with different values of the average concentration of D atoms are shown in Fig. 10. Error bars correspond to the scattering of line width values for fitting curves used to simulate shape of the hyperfine components. Typically, 90% of the D atom population corresponded to the broad Lorentzian and the remained 10% corresponded to the narrow Lorentzian. There were correlations of the line widths of each Lorentzian with the average concentration values obtained for the samples under study (Fig. 10). We can see a change of slope for the line width dependencies of both Lorentzians at the average concentration $2\cdot10^{19}$ cm^{-3} is accompanied by the appearance of a sharp Gaussian in the next point, at $3.3\cdot10^{19}$ cm^{-3} (Fig. 9). A very small fraction of the D atoms (~1%) corresponded to a Gaussian component. We therefore suggest that a change of slope for the line width dependences depicted in Fig. 10 could be a manifestation of exchange narrowing. This

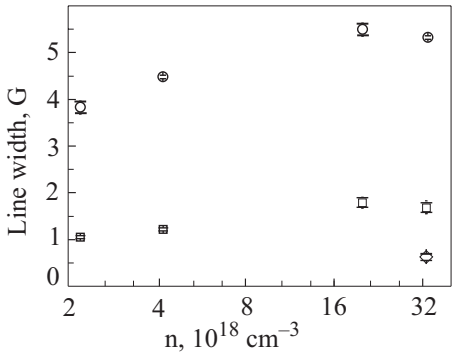

Fig. 10. Line widths of fitting curves for Kr–He nanocondensates for different values of the average concentration of D atoms: broad Lorentzian (○), narrow Lorentzian (□), sharp Gaussian (◇).

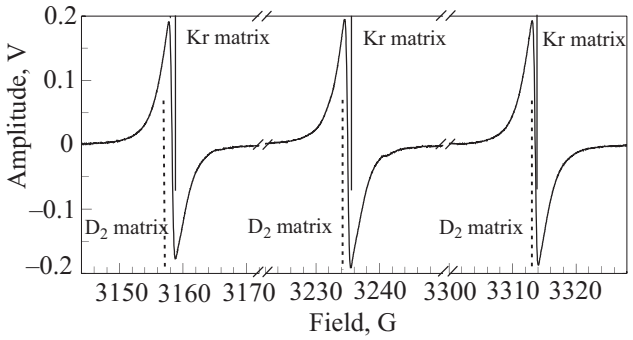

Fig. 11. ESR spectra of D atoms in as-prepared Kr–He sample at 1.35 K. Sample was prepared from a gas mixture with the ratio [HD]:[Kr]:[He] = 1:5:1200. Dashed and solid lines correspond to the hyperfine line positions of D atoms stabilized in D_2 and Kr matrices, respectively.

provides a motivation for further experiments on samples with the highest D atom concentrations.

It is worth noting that no recombination of D atoms has been observed at 1.35 K for any of the Kr–He samples studied in spite of the high atomic densities reached. Therefore the deuterium atoms are completely localized on the nanocluster surfaces in Kr–He samples.

3.3. H and D atoms in krypton–helium condensates

Finally, we discuss experimental results obtained for two Kr–He samples prepared from gas mixtures initially containing HD, Kr and He in the ratios [HD]:[Kr]:[He] = = 1:5:1200 and [HD]:[Kr]:[He] = 1:50:10,000. Henceforth these samples will be called sample #1 and sample #2. Surprisingly we have observed changes of ESR spectra of H atoms stabilized in these as-prepared samples in comparison with the case for samples prepared from $[H_2]$:[Kr]:[He] gas mixtures while ESR spectra of the D atoms were similar to those obtained for samples formed by $[D_2]$:[Kr]:[He] gas mixtures (Fig. 11). The positions of fitting curves for spectra of D atoms lie in the ranges between magnetic field values corresponding to matrices of molecular deuterium and krypton. As one can see in Fig. 11 the low field hyperfine component of the ESR spectra (Fig. 11) is the most sensitive component to the changes of the hyperfine splitting constant and/or g-factor values of D atoms.

As before, ESR spectra of H atoms were fitted by three curves (Fig. 12), but the fitting curve positions coincided within 0.2 G just as for the case of D atoms, and the bump on LFL («fingerprints» of H atoms stabilized inside Kr clusters) has disappeared. As a consequence, the values of the hyperfine splitting constant and *g*-factor were almost

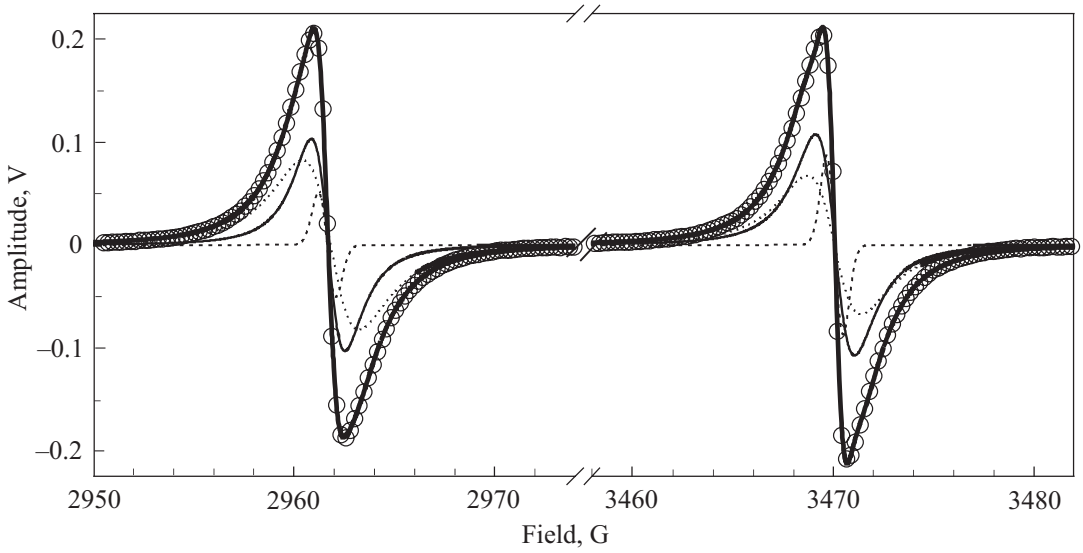

Fig. 12. ESR spectra (○) of H atoms in as-prepared Kr–He sample at 1.35 K. Sample was prepared from a gas mixture with the ratio [HD]:[Kr]:[He] = 1:5:1200. Gaussians are dashed lines, broad and narrow Lorentzians are dotted and thin lines, respectively, and the sums of fitting curves are thick lines. A bump is not observed in these spectra.

Table 3. Hyperfine structure constants, A, g-factors and line widths for H and D atoms in the as-prepared Kr–He samples

Atoms, sample, fitting curve	A, MHz	$\Delta A/A_{free}$, %	g-factor	Line width, G
H, sample #1, Gaussian	1415.43	–0.35	2.00209	0.9
H, sample #1, broad Lorentzian	1414.73	–0.4	2.00208	4.8
H, sample #1, narrow Lorentzian	1415.41	–0.35	2.00207	3.1
H, sample #2, Gaussian	1414.75	–0.4	2.00203	0.8
H, sample #2, broad Lorentzian	1414.02	–0.45	2.00203	3.75
H, sample #2, narrow Lorentzian	1414.51	–0.415	2.00193	1.92
D, sample #1, broad Lorentzian	217.491	–0.35	2.00192	4.5
D, sample #1, narrow Lorentzian	217.486	–0.35	2.00194	1.3
D, sample #2, broad Lorentzian	217.407	–0.39	2.00189	3.83
D, sample #2, narrow Lorentzian	217.4207	–0.38	2.00194	1.05

the same for all the fitting curves (Table 3) as if all H and D atoms are distributed over the same region on the krypton clusters.

The solid films on the Kr nanocluster surfaces are expected to contain H and D atoms, He atoms, and D_2 and HD molecules. The ingredients for the exchange tunneling reactions $D + H_2 \rightarrow HD + H$ and $D + HD \rightarrow D_2 + H$ to take place on the cluster surfaces are therefore present.

Figure 13 shows the time evolution of the H and D populations of both mixed samples. Sample #1 (solid symbols in Fig. 13) does indeed show an increase in the H atom population and a decrease in the D atom population over time. This is the signature of the above tunneling reactions. There is no hint of any tunneling reaction occurring in sample #2. We detected ESR signals from $\approx 7.4\cdot10^{17}$ H atoms and $\approx 7.7\cdot10^{17}$ D atoms, about 25% of the H and D atoms produced during preparation of sample #2 (a total of $\approx 3\cdot10^{18}$ HD molecules were dissociated in gas jet). In this case there were a couple of molecules only per atom (H or D) and no way to migrate through the solid environment of krypton clusters. From similar estimations for sample #1 there were more molecules (up to 9–10) per H or D atom (ESR signals were detected from $1.1\cdot10^{18}$ and $1.5\cdot10^{18}$ of H and D atoms, respectively, or about 5 % of the atoms produced during sample preparation),

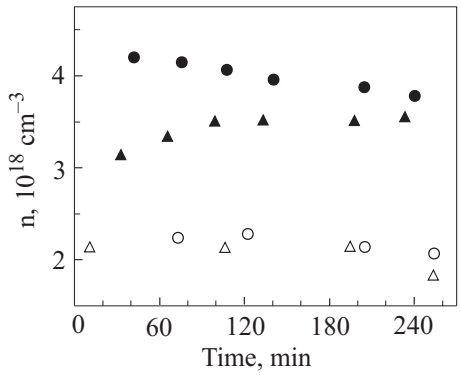

Fig. 13. Time dependences of H (triangles) and D (circles) atom concentrations in HD–Kr–He samples prepared from the gas mixtures: [HD]:[Kr]:[He] = 1:5:1200 — solid symbols, [HD]:[Kr]:[He] = 1:50:10,000 — open symbols.

the number of molecules is not enough to form a matrix without involving the krypton cluster surfaces and He atoms. Such an inhomogeneous environment definitely restricts the mobility of hydrogen atoms, keeping the reaction rate small:

Moreover, there is another interesting point for sample #1. The sums of the initial and final populations of H and D atoms have a constant value:
at the beginning

$$n_H + n_D = 3.1\cdot10^{18}\ \text{cm}^{-3} + 4.2\cdot10^{18}\ \text{cm}^{-3} = 7.3\cdot10^{18}\ \text{cm}^{-3};$$

at the end

$$n_H + n_D = 3.5\cdot10^{18}\ \text{cm}^{-3} + 3.8\cdot10^{18}\ \text{cm}^{-3} = 7.3\cdot10^{18}\ \text{cm}^{-3}$$

indicating the absence of recombination.

The absence of recombination also can be associated with almost complete localization of H and D atoms. Therefore they could interact with nearest neighbor molecules only and could not migrate through the solid film on the krypton cluster surfaces.

The observation of tunneling reactions in the sample prepared from [HD]:[Kr]:[He] gas mixtures has allowed us to obtain some information regarding the distribution of H and D atoms over the Kr–He sample. The portion of H atoms corresponding to the broad Lorentzian corresponds to the same location as that for the D atoms: the growth of H atom population leads to increasing the number of H atoms corresponding to the broad Lorentzian and compensates for the drop of D atom population described by depletion of D atoms corresponding to the broad Lorentzian (90%) mainly and the narrow Lorentzian (10%). Two other populations of the H atoms do not participate in the reaction. A possible reason is that the atoms have slightly different environments (it is confirmed by slightly different values of the hyperfine structure constants 1415.43 and 1415.45 MHz versus 1414.73 MHz). The H–D system is rather complex and will require further experiments to gain a better understanding.

Summary

Upon condensation of Kr atoms with light hydrogen isotopes, most of the light atoms are stabilized on the surfaces of krypton nanoclusters. The average concentrations of H and

D atoms in this system are considerably larger than those obtained for samples containing only hydrogen isotopes [35]. Very high average concentrations, $1.2 \cdot 10^{19}$ cm^{-3} for H atoms and $3.3 \cdot 10^{19}$ cm^{-3} for D atoms, have been obtained. For the latter case the narrowing of ESR lines was observed. There are some potential ways for further increasing the energetic content of IHCs containing H and D atoms: firstly, a determination of optimal ratio for gas mixture used to prepare such samples; secondly, a sample shrinkage at annealing as well as a simple mechanical compression of a sample should lead to an increase in the energy density up to one order of magnitude due to the high porosity of the IHCs; finally, a good choice of heavy impurity can bring additional energy into the system.

The high densities of deuterium (hydrogen) atoms (with their unpaired electron spins) on the cluster surfaces may exhibit interesting magnetic properties. We observed narrowing of ESR lines of deuterium atoms stabilized in the Kr–He sample with the highest density of D atoms ($3.3 \cdot 10^{19}$ cm^{-3}) obtained in these experiments. Introducing liquid ^{3}He into the pores of a Kr–He sample containing large surface concentrations of D (or H) atoms provides the opportunity to study the interactions between their electron spins and the nuclear moments of ^{3}He.

An observation of tunneling reactions in the sample prepared from [HD]:[Kr]:[He] gas mixture has allowed us to obtain information on the distribution of H and D atoms over a Kr–He sample. It is worth noting the "isotopic" effect in the distribution of atoms over the Kr–He samples. Deuterium atoms localized on surface of krypton nanoclusters exclusively, whereas hydrogen atoms were partially embedded inside the clusters. It is also interesting to note that we were not able to detect H atoms inside krypton clusters forming the Kr–He samples prepared from [HD]:[Kr]:[He] gas mixtures.

Acknowledgments

This work was supported by National Science Foundation Grant DMR 0504683. The authors are grateful to E.P. Bernard and J. Järvinen for participation in the experiments, and to I.N. Krushinskaya for help in data analysis.

1. P. Savich and A. Shalnikov, *J. Phys. USSR* **10**, 299 (1946).
2. J. Jortner, L. Meyer, S.A. Rice, and E.G. Wilson, *Phys. Rev. Lett*. **12**, 415 (1964).
3. M. Himbert, A. Lezama, and J. Dupont-Roc, *J. Phys*. **46**, 2009 (1985).
4. B. Tabbert, H. Gunther, and G. zu Putlitz, *J. Low Temp. Phys*. **109**, 653 (1997).
5. P. Moroshkin, A. Hofer, and A. Weis, *Phys. Rep*. **469**, 1 (2008).
6. J.P. Toennies and A.F. Vilesov, *Annu. Rev. Phys. Chem.* **49**, 1 (1998).
7. F. Stienkemeier and K.K. Lehmann, *J. Phys*. **B39**, R127 (2006).
8. A.M. Bass and H.P. Broida, *Formation and Trapping of Free Radicals*, Academic Press, New York and London (1960).
9. G.W. Collins, J.L. Maienschein, E.R. Mapoles, R.T. Tsugawa, E.M. Fearon, P.C. Souers, J.R. Gaines, and P.A. Fedders, *Phys. Rev*. **B48**, 12620 (1993).
10. J. Ahokas, O. Vainio, J. Jarvinen, V.V. Khmelenko, D.M. Lee, and S. Vasiliev, *Phys. Rev*. **B79**, 220505 R (2009).
11. E.B. Gordon, L.P. Mezhov-Deglin, and O.F. Pugachev, *JETP Lett.* **19**, 103 (1974).
12. R.E. Boltnev, E.P. Bernard, J. Jarvinen, V.V. Khmelenko, and D.M. Lee, *Phys. Rev*. **B79**, 180506 R (2009).
13. R.E. Boltnev, E.P. Bernard, J. Jarvinen, I.N. Krushinskaya, V.V. Khmelenko, and D.M. Lee, *J. Low Temp. Phys*. **158**, 468 (2010).
14. E.B. Gordon, A.A. Pelmenev, O.F. Pugachev, and V.V. Khmelenko, *JETP Lett*. **37**, 282 (1983).
15. E.B. Gordon, V.V. Khmelenko, A.A. Pelmenev, E.A. Popov, and O.F. Pugachev, *Chem. Phys. Lett*. **156**, 301 (1989).
16. G. Breit and I.I. Rabi, *Phys. Rev*. **38**, 2082 (1931).
17. V. Kiryukhin, B. Keimer, R.E. Boltnev, V.V. Khmelenko, and E.B. Gordon, *Phys. Rev. Lett*. **79**, 1774 (1997).
18. V. Kiryukhin, E.P. Bernard, V.V. Khmelenko, R.E. Boltnev, N.V. Krainyukova, and D.M. Lee, *Phys. Rev. Lett*. **98**, 195506 (2007).
19. R.E. Boltnev, I.N. Krushinskaya, A.A. Pelmenev, E.A. Popov, D.Yu. Stolyarov, and V.V. Khmelenko, *Fiz. Nizk. Temp.* **31**, 723 (2005) [*Low Temp. Phys*. **31**, 547 (2005)].
20. N.V. Krainyukova, *Thin Solid Films* **515**, 1658 (2006).
21. J. Jarvinen, E.P. Bernard, R.E. Boltnev, V.V. Khmelenko, and D.M. Lee, *J. Phys.: Conf. Ser*. **150**, 03235 (2009).
22. S.I. Kiselev, V.V. Khmelenko, and D.M. Lee, *Phys. Rev. Lett*. **89**, 175301 (2002).
23. R. Beringer and M.A. Heald, *Phys. Rev*. **95**, 1474 (1954).
24. P. Kusch, *Phys. Rev*. **110**, 1188 (1955).
25. C.K. Jen, S.N. Foner, E.L. Cochran, and V.A. Bower, *Phys. Rev*. **104**, 846 (1956).
26. S.N. Foner, E.L. Cochran, V.A. Bower, and C.K. Jen, *J. Chem. Phys*. **32**, 963 (1960).
27. Yu.A. Dmitriev, *Fiz. Nizk. Temp.* **33**, 661 (2007) [*Low Temp. Phys*. **33**, 493 (2007)].
28. K. Vaskonen, J. Eloranta, T. Kiljunen, and H. Kunttu, *J. Chem. Phys*. **110**, 2122 (1999).
29. W. Gordy, and R. Morehouse, *Phys. Rev*. **151**, 207 (1966).
30. A.G. Prodell and P. Kusch, *Phys. Rev*. **79**, 1009 (1950).
31. A.G. Prodell and P. Kusch, *Phys. Rev*. **88**, 184 (1952).
32. C.K. Jen, S.N. Foner, E.L. Cochran, and V.A. Bowers, *Phys. Rev*. **112**, 1169 (1958).
33. E.P. Bernard, R.E. Boltnev, V.V. Khmelenko, V. Kiryukhin, S.I. Kiselev, and D.M. Lee, *Phys. Rev*. **B69**, 104201 (2004).
34. L.B. Knight, Jr., W.E. Rice, L. Moore, E.R. Davidson, and R.S. Dailey, *J. Chem. Phys*. **109**, 1409 (1998).
35. V.V. Khmelenko, E.P. Bernard, S. Vasiliev, and D.M. Lee, *Russ. Chem. Rev*. **76**, 1107 (2007).